applied sciences

MDPI

Article

GEOBIA and Vegetation Indices in Extracting Olive Tree Canopies Based on Very High-Resolution UAV Multispectral Imagery

Ante Šiljeg [1,*], Rajko Marinović [1], Fran Domazetović [1], Mladen Jurišić [2], Ivan Marić [1], Lovre Panđa [1], Dorijan Radočaj [2] and Rina Milošević [1]

[1] Department of Geography, University of Zadar, Trg Kneza Višeslava 9, 23000 Zadar, Croatia
[2] Faculty of Agrobiotechnical Sciences, Josip Juraj Strossmayer University of Osijek, 31000 Osijek, Croatia
* Correspondence: asiljeg@unizd.hr

Abstract: In recent decades, precision agriculture and geospatial technologies have made it possible to ensure sustainability in an olive-growing sector. The main goal of this study is the extraction of olive tree canopies by comparing two approaches, the first of which is related to geographic object-based analysis (GEOBIA), while the second one is based on the use of vegetation indices (VIs). The research area is a micro-location within the Lun olives garden, on the island of Pag. The unmanned aerial vehicle (UAV) with a multispectral (MS) sensor was used for generating a very high-resolution (VHR) UAV_{MS} model, while another mission was performed to create a VHR digital orthophoto (DOP). When implementing the GEOBIA approach in the extraction of the olive canopy, user-defined parameters and classification algorithms support vector machine (SVM), maximum likelihood classifier (MLC), and random trees classifier (RTC) were evaluated. The RTC algorithm achieved the highest overall accuracy (OA) of 0.7565 and kappa coefficient (KC) of 0.4615. The second approach included five different VIs models (NDVI, NDRE, GNDVI, MCARI2, and RDVI2) which are optimized using the proposed VITO (VI Threshold Optimizer) tool. The NDRE index model was selected as the most accurate one, according to the ROC accuracy measure with a result of 0.888 for the area under curve (AUC).

Keywords: geospatial technologies; Lun olive groves; object-based image analysis; classification algorithms; machine learning; accuracy assessment

check for updates

Citation: Šiljeg, A.; Marinović, R.; Domazetović, F.; Jurišić, M.; Marić, I.; Panđa, L.; Radočaj, D.; Milošević, R. GEOBIA and Vegetation Indices in Extracting Olive Tree Canopies Based on Very High-Resolution UAV Multispectral Imagery. *Appl. Sci.* **2023**, *13*, 739. https://doi.org/10.3390/app13020739

Academic Editor: Krzysztof Koszela

Received: 29 November 2022
Revised: 28 December 2022
Accepted: 31 December 2022
Published: 4 January 2023

Copyright: © 2023 by the authors. Licensee MDPI, Basel, Switzerland. This article is an open access article distributed under the terms and conditions of the Creative Commons Attribution (CC BY) license (https://creativecommons.org/licenses/by/4.0/).

1. Introduction

The olive tree is one of the oldest species in the Mediterranean area [1–3] which has been spreading throughout history and shaped the recognizable Mediterranean landscape [4,5]. Resistance to extreme climatic conditions and adaptability to different types of poorly fertile soils ensure the olive's social, ecological, and economic benefits [6,7]. Sustainability and preservation of olive trees are especially important [8] due to the frequent impacts of various economic activities such as industry, wildfires [9], and tourism sector activities [10,11]. Preservation mostly depends on sustainable environmental management and precision agriculture (PA) methodologies [12–15]. Geospatial technologies and their products have become easily available and widely accessible in everyday life, which has advanced and accelerated their use in various research [16–19]. The development of advanced geospatial technologies has enabled PA in the olive management sector, especially in the context of precise canopy extraction for management [20–22], monitoring [23–25], assessment of crop quality [26], disease detection [27], and preventive actions [28]. Therefore, geospatial technologies have a meaningful role in the observation and analysis of various processes located on the Earth's surface.

Unmanned aerial vehicles (UAVs) are objects that can be controlled remotely or have a pre-set programmed flight plan [29,30], and their main advantage is the competency

to collect very high spatial resolution data [31,32]. The use of UAVs has become necessary for most scientists in terms of collecting high spatial resolution data necessary for conducting interdisciplinary research [33–35]. UAVs have been applied significantly for remote sensing of vegetation and natural regions. UAV-based RS applications provide considerably better resolution and more flexibility in choosing acceptable payloads and appropriate spatiotemporal resolution than satellite-based RS applications [36]. Due to the enhancement of geomorphic elements over the landscape, the creation of UAV-derived datasets, such as orthomosaics and high-resolution digital elevation models, enables the characterization and geometrical analysis of the channels, improving their identification in areas with vegetation [37]. In the process of remote sensing, multispectral (MS) sensors are one of the most powerful tools for a better understanding of environmental processes [38]. Moreover, they are one of the most frequently used sensors, which was primarily influenced by their exceptional applicability in forestry, PA, and other economic activities that are closely related to vegetation [34]. MS sensors provide insight into the part of the electromagnetic spectrum that is invisible to the human eye, and in terms of remote sensing, they represent a significant contribution with the aim of better understanding environmental processes [38,39]. MS sensors play a leading role in PA, mostly due to the possibility of extracting vegetation indices (VIs) [40].

VIs are one of the more widely used indicators within the geospatial analysis and PA [13,41,42] and are defined as the result of a combination of two or more spectral bands [43–45]. Analysis of VIs is generally performed with the use of MS sensors, enabling the classification of the study area based on spectral characteristics [46,47]. VIs are primarily used to distinguish observed crops or analyze the canopies of various plants [15,48]. A lot of authors use VIs in order to reach some new knowledge and conclusions regarding the vegetation in agriculture sectors. In [48], three VIs (GNDVI, NDVI, SAVI) is used to monitor the vegetation phases of vineyard and tomato crops. In [19] for PA, five VIs models (NDVI, GNDVI, SAVI, BNDVI, GSAVI) are derived to extract the chestnut canopies. In [13], WorldView-3 satellite imagery is used to extract and analyze VIs inside olive tree canopies.

Classifications of observed surfaces can be performed using various methods, and apart from the mentioned approach based on VIs, still, the most used approach is related to geographic object-based analysis (GEOBIA) [49,50]. GEOBIA is defined as a subdiscipline of geographic information systems (GIS) focused on the processing and analysis of raster data [51]. Unlike pixel-based analyses, GEOBIA groups pixels into meaningful homogeneous units according to their spectral characteristics [49]. The main difference between the VIs approach and GEOBIA is the different use of MS images and the data they contain. VIs use pixel information to create certain VI model, which is later processed within the VITO tool. On the other hand, GEOBIA requires the use of randomly selected training samples to gather data about the landscape in order to successfully carry out the classification. Sometimes, the accuracy might well be determined only by the selection of inadequate training samples. Comparison and accuracy assessment of olive trees canopy extraction based on VIs and the GEOBIA approach is important in PA, intending to improve the sustainable management of olive groves and other plants with similar vegetative characteristics.

Other methods in the process include deep learning classifier, which success is based on deep neural networks (DNN) [52]. Deep learning is a computer-based modeling technique that consists of numerous processing layers and is used to comprehend how data is represented at various levels of abstraction [53]. It is still debatable whether or to what extent deep learning techniques can outcompete other state-of-the-art and support vector machine (SVM) algorithms in the context of classification using GEOBIA, despite the recent explosion in popularity of DNNs [54]. Although a deep learning classifier was not utilized in this study, it will undoubtedly be considered in future research.

The main goal of this research is to compare the accuracy in the extraction of olive tree canopies between the GEOBIA approach and the approach based on VIs. The secondary objectives are to determine the best of the three tested classification algorithms in the

GEOBIA approach and to optimize and select the most representative VI to extract the olive tree canopy.

2. Materials and Methods

2.1. Study Area

The study area for the comparison of two approaches when extracting olive tree canopies is a micro-location within the area of the Lun olive gardens. The Lun olive groves are positioned in the northwestern part of the island of Pag, in the immediate vicinity of the Lun settlement (Figure 1). Lun olive garden is one of the most valuable natural phenomena on the island of Pag, and in 1963 the area was entered into the register of protected natural objects and declared a botanical reserve. The thousand-year-old wild olives within the research area are part of the "Natura 2000" ecological network. More than 80 thousand trees, spread over about 24 hectares, represents a very rarely seen phenomenon in the world since thousand-year-old olive trees are mostly found alone or in smaller groups [55].

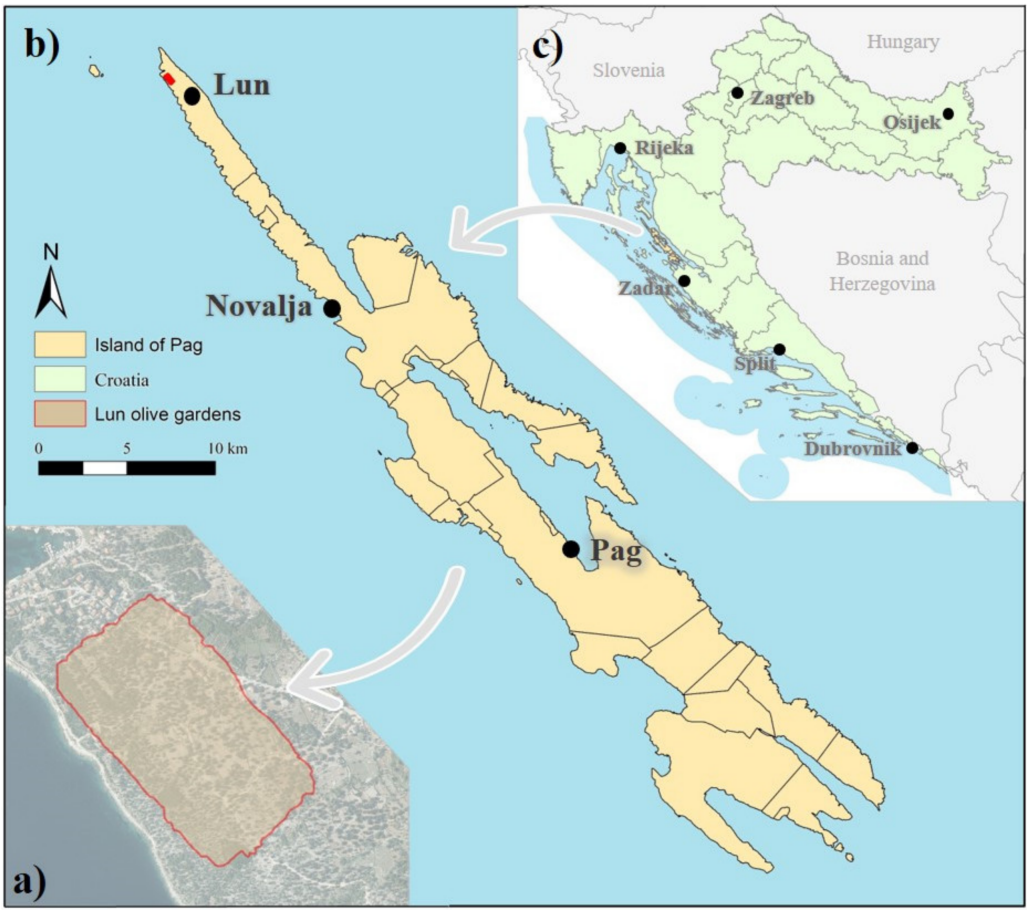


Figure 1. Study area: (**a**) Test area in Lun olive gardens; (**b**) island of Pag; (**c**) Croatia.

2.2. The Methodological Framework

The research methodology comprises the next steps: field research and data collection (1); creation of UAV_{MS} and digital orthophoto (DOP) (2); the GEOBIA analysis (3), the proposed method based on VIs (4); approaches accuracy assessment comparison (5) (Figure 2).

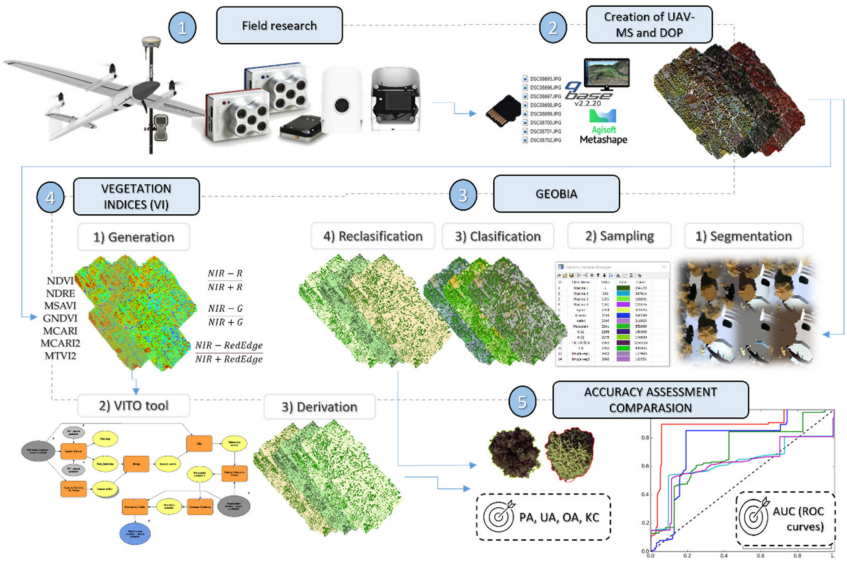


Figure 2. The research methodology framework.

2.3. Field Research

The field research was conducted on 19 October 2021. Aerial photogrammetry was carried out in this part of the year because at that time the olives enter the stage of maturity, during which all the branches have a similar reflection. The second reason relates to the pruning of olive trees, which most often takes place in the winter period [56]. Two aerial photogrammetry missions were conducted for this study. The first mission included the use of the MicaSense RedEdge-MX Dual MS camera (Table 1), while the Sony RX1R II RGB sensor was used in the second mission. Both sensors are mounted as an integral part of the Trinity F90+ UAV, which provides excellent capabilities in terms of imaging and collecting data from very large and inaccessible areas. In addition to the mentioned geospatial technology, RTK GNSS Trimble R8s was used to collect checkpoints (CP) and reference points (RP).

Table 1. MicaSense RedEdge-MX Dual MS specifications.

Sensor Type	Multispectral (MS)
Spectral Bands	Coastal blue (444 nm), blue (475 nm), green (531 nm), green (560 nm), red (650 nm), red (668 nm), red edge (705 nm), red edge (717 nm), red edge (740 nm), near-infrared (842 nm)
Ground Sample Distance	8 cm per pixel (per band) at 120 m

2.4. Data Acquisition

Before any UAV imaging, the first step of data acquisition involved marking and collecting CP and RP on a local geodetic basis. A total amount of 7 CPs were collected, which were used to check the accuracy of the UAV's direct georeferencing system. The RPs where the UAV's positioning device or base station iBase was placed, were also collected. All points were measured in the official projection coordinate system of the Croatian Terrestrial Reference System (HTRS96/TM). The next step was related to the planning of the UAV missions, which was carried out using the QBase 3D software (Figure 3). MS imaging mission was carried out with a front and side overlap of 70%, while considering the terrain morphology and the desired level of detail, the relative flight altitude was set to 100 m. Settings provided a ground sampling distance (GSD) for the UAV_{MS} of 6.94 cm/px (Figure 3). On the other hand, the settings of the second mission related to the RGB sensor were set to front and side overlap of 75% and the relative flight altitude of 140 m. The

expected GSD for DOP was 1.81 cm/px. Before the flight, the process of calibration of the UAV's initial measurement systems (IMUs) was carried out, followed by the radiometric calibration of the MS sensor, using the appropriate reference calibration panel. After the processes, aerial photogrammetric imaging of the selected research area was performed. The radiometric calibration of the MS sensor was repeated after a mission to determine any differences in the atmospheric conditions.



Figure 3. Field work; (**a**) Trinity F90+ MS mission; (**b**) Trimble R8s CPs and RP collecting.

2.5. UAV Imagery Processing

Images were primarily geocoded using UAV's Flylog records and the data from the base station. Then, MS and RGB images were processed using Agisoft Metashape 1.5.11, which was mostly used because of the implemented structure-from-motion (SfM) and 3D modeling algorithms based on overlapping 2D images. After a series of appropriate settings and steps such as photo orientation, creation of a dense cloud of points, deep filtering, and optimization of sensor locations, a 3D model was obtained and exported as UAV_{MS} and DOP.

2.6. GEOBIA

2.6.1. MS Bands Layout

The selection of the MS bands layout depends on the type and characteristics of the vegetation that is selected [13]. Coastal blue and blue bands are significant for coastal applications, such as deep-water masks differentiation or water body penetration. The green band is applicable for distinguishing crop types and bathymetry, while the yellow band is intended for leaf coloration, plant stress, or separability of iron formations. The red band is used for the detection of chlorophyll absorption or plant species and stress. Various red edge bands are commonly used to detect vegetation health and stress, while the near-infrared band is preferred for biomass surveys, type and age discrimination, and plant stress detection. Since the objects of this research are olive tree canopies, the selection of band arrangement is conditioned by the spectral reflectance of olive trees which is the best in all bands except blue ones. Therefore, when choosing the band layout, various combinations were visually compared.

2.6.2. Segmentation

The second step in the GEOBIA process of extracting olive tree canopies is segmentation, a process based on the Mean shift approach implemented in ArcGIS. The Segment Mean Shift tool identifies the characteristics or segments in images by clustering pixels with similar spectral, spatial, and geometrical characteristics. The image segment characteristics are determined by the spectral detail, the spatial detail, and the minimum size of the segment. An iterative process was used to optimize the values of the aforementioned parameters (n = 42). Based on the visual interpretation of the UAV_{MS} segmentation results, the best combination of parameter values was chosen (Figure 4).

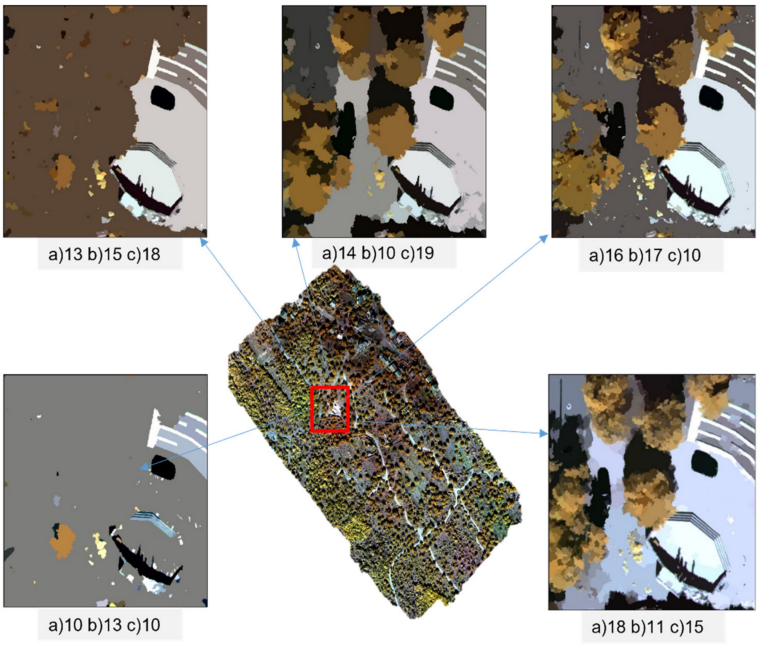


Figure 4. Differences between various segmented models: (**a**) spectral detail; (**b**) spatial detail; (**c**) minimum segment size.

2.6.3. Test Samples

The third step refers to adding test samples to the segmented model. Select Segment tool within the Training Sample Manager was used to add samples. When adding, the appropriate number of classes that will represent the research object, as well as the number of other classes within the observed area, is optimized. The research object, i.e., the olive tree canopies, was collected within four classes (Figure 5), mostly due to the morphology and the solar incidence angle, which caused differences in the spectral reflection within the canopies.

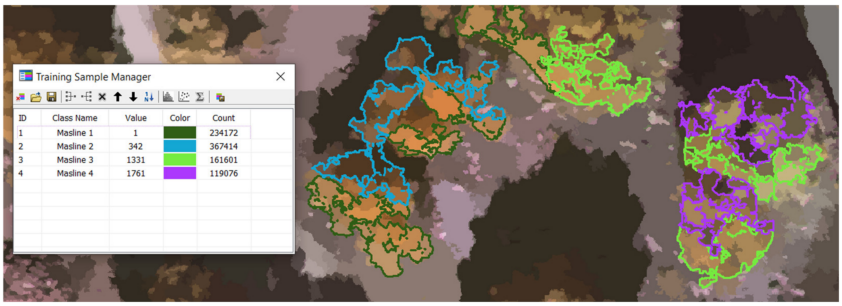


Figure 5. Adding olive tree class samples.

2.6.4. Classification

Classification of the segmented footage was performed using three classification algorithms: (1) Support vector machine (SVM), (2) maximum likelihood classifier (ML), and (3) random trees classifier (RTC). Models were classified into 14 classes and then reclassified into "olive tree canopies" and "other classes. Details on each classification algorithm and its conduct in the classification process are discussed in Sections 3.2.3 and 3.2.4.

2.6.5. Accuracy Assessment

The GEOBIA process was concluded with the selection of the most accurate classification algorithm. Accuracy assessment was performed using producer accuracy (*PA*), user accuracy (*UA*), overall accuracy (*OA*), and kappa coefficient (*KC*) measures. *PA* represents the likelihood that a reference pixel was correctly classified, whereas *UA* represents the

likelihood that a classified pixel represents that class on the ground [57]. The quotient of the total number of correct pixels and the total number of pixels in the error matrix is represented by *OA* [58,59], while *KC* represents a measure of the relationship between classified and reference data, shown by the confusion matrix's main diagonal, and by random matching represented by the sums of the columns and rows of the matrix [60,61]

$$PAi = \frac{Pii}{P+i} \quad (1)$$

$$UAi = \frac{Pii}{Pi+} \quad (2)$$

$$\mathrm{OA} = \sum_{i=1}^{m} Pii \quad (3)$$

$$KC = \frac{N\sum_{i=1}^{r} Pii - \sum_{i=1}^{r}(p_{i+} * p_{+i})}{N^2 - \sum_{i=1}^{r}(p_{i+} * p_{+i})} \quad (4)$$

where p_{ii} represents the major diagonal element for class I, p_{i+1} represents the total number of observations in column I (bottom margin), p_{i+} represents the total number of observations in row I (right margin), and m represents the number of rows and columns in the error matrix. *PA*, *UA*, and *OA* values range from 0 to 1. A higher value indicates greater precision. Accuracy assessment was performed using layers of regularly spaced points generated within polygons representing reference trees (RT) and false trees (FT). This method ensures hundreds of thousands of samples are positioned within the RT and FT, insuring the most accurate results [62,63].

The first step involved the vectorization of nine RT and nine FT from very high-resolution DOP (Figure 6a,b). The next step involved creating a point layer for each pixel, i.e., fishnet within the RT and FT polygons (Figure 6c). Furthermore, for each point, an attribute is added within the attribute table, which refers to the actual value of the point on the ground (0 or 1) (Figure 6d). Validation polygons were created using VHR DOP with a spatial resolution of 1.88 cm.

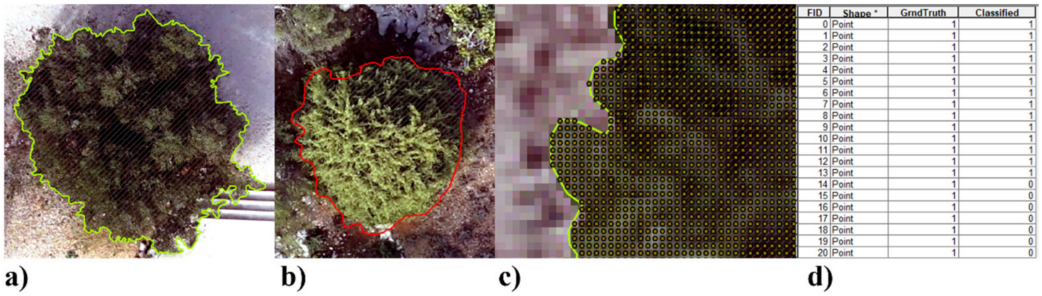


Figure 6. Accuracy assessment steps: (**a**) RT vectorization; (**b**) FT vectorization; (**c**) fishnet; (**d**) attribute table.

2.7. Vegetation Indices (VI)

VIs were generated using a Raster calculator tool within ArcGIS, which allows the input of different spectral bands into the corresponding formula of the VI.

2.7.1. VITO Tool

The proposed VITO (vegetation index threshold optimizer) tool was created to automate the process to separate olive tree canopies using selected VIs. As input data, the VITO tool primarily uses previously vectorized polygons of olive tree canopies. First, by using the Feature vertices to Points tool, the breaking points of the olive canopies are extracted. This layer of points represents the outer part of the olive tree canopy, while the inner part is generated with the Create Fishnet tool, as a layer of regularly spaced points. Both sets of point layers are prepared for merging as they represent reference samples for the second

part of the tool. On the other side of the tool scheme, the VITO tool uses a chosen VI model as input data, after which the model values are added to the recently merged layer of points. To utilize the Reclass by Table tool, which uses statistics to produce output results in the form of classified olive tree canopies, all extracted data is documented in the form of a table, using the Summary Statistics tool. After the reclassification process, the final result of the VITO tool is extracted olive tree canopies (Figure 7).

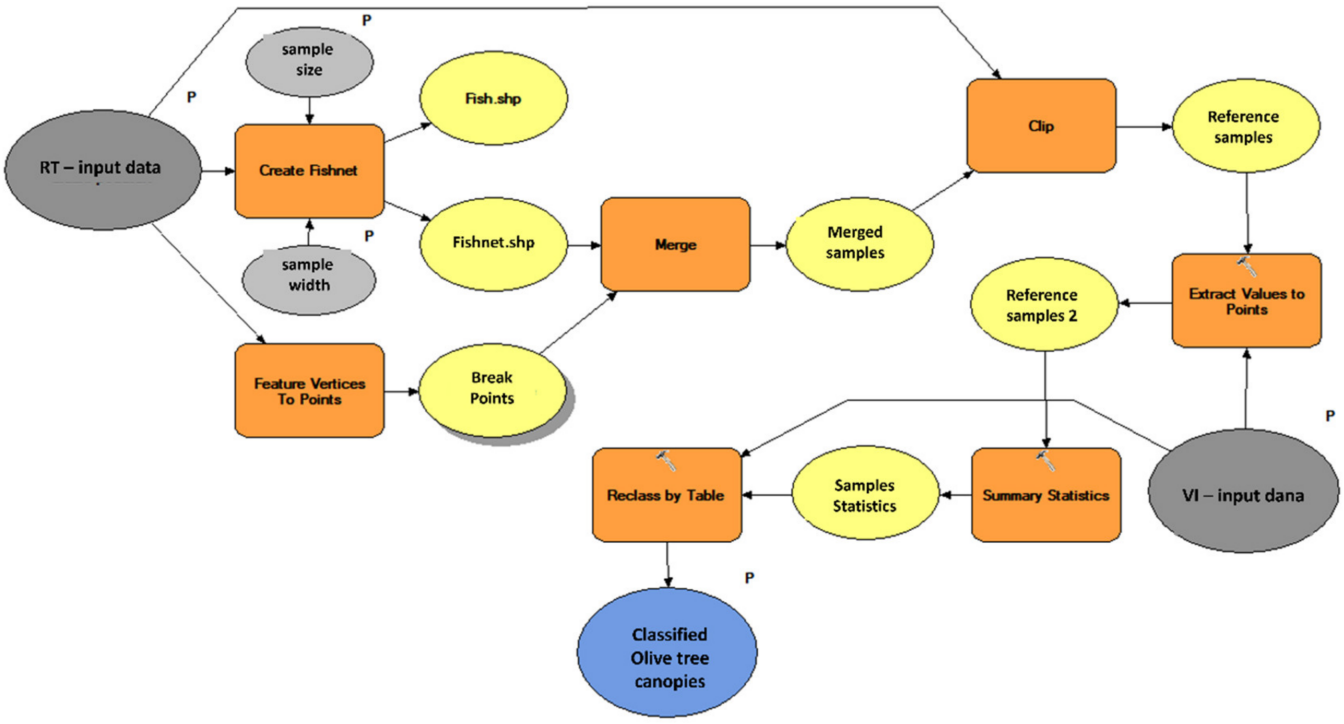


Figure 7. VITO tool scheme.

2.7.2. Accuracy Assessment

The accuracy of the VIs olive tree canopies models was accessed using AUC (area under the curve) values obtained from ROC (receiver operating characteristics) curves. ROC curve is a graphic diagram that illustrates the diagnostic ability of a certain classifier system, and it is created using TRP (true-positive rate) and FPR (false-positive rate) values of the observed model [64,65]. ROC curves are commonly calculated by either utilizing the design sample reuse approach or by applying the classification rule to a test set of points with known classes. While the AUC represents the possibility that a randomly selected member of class 1 will have a lower estimated chance of being a member of class 0 than a randomly selected member of class 0 [66]. ROC or AUC are often used wherever it is necessary to verify or visualize the performance of multi-class classifications [67]. The creation of ROC curves and AUC values is a fully automated process using the Calculate ROC Curves and AUC Value tool, which was integrated into ArcGIS within the ArcSDM Tools set.

2.8. Comparison of Classification Approaches

The first way of implementing accuracy measures to compare approaches included layers of regular distribution of points (fishnet) within polygons of RT and FT. Polygons were evenly distributed within the research area (Figure 8), to reduce the possibility of error and obtain the most accurate results. The tools Compute Confusion Matrix and Calculate ROC Curves and AUC Values within ArcGIS created confusion matrices and ROC curves for each of the two approaches.

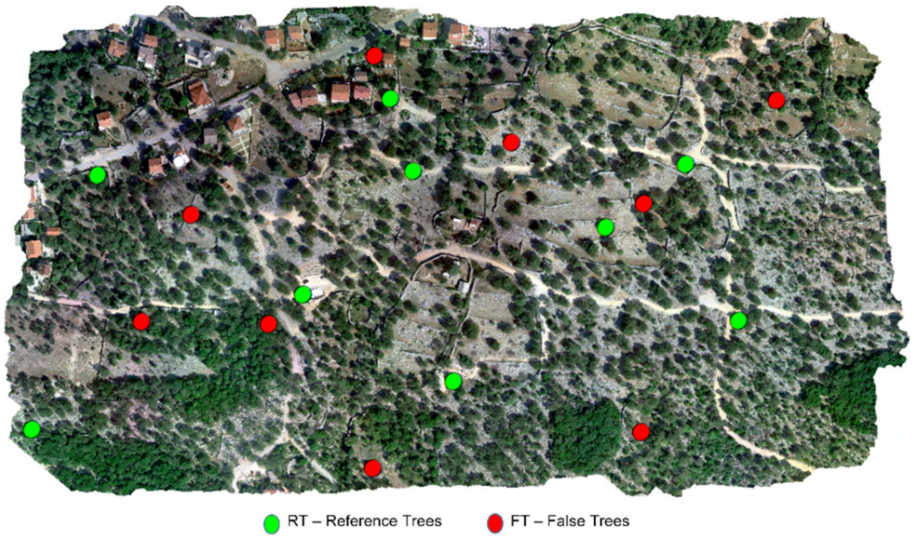


Figure 8. Distribution of RT and FT.

The second way of comparison was carried out using a layer of one thousand randomly distributed points (Figure 9) created using the Create Accuracy Assessment Points tool. Points are also randomly distributed within the research area. For each point, based on the very high-resolution reference DOP, an attribute was added that indicates the real belonging to the class in space, i.e., 0 for the other class and the value 1 if the point in the research area is inside the olive tree canopy. Using the same tools as in the first comparison method, confusion matrices and ROC curves were created, which contain the results of the accuracy measures used.



Figure 9. Thousand randomly distributed accuracy assessment points.

3. Results and Discussion

3.1. UAV-MS and DOP Creation

With the MS sensor, a total of 4840 images were taken. The images were collected from 484 locations, considering that the MicaSense RedEdge-MX Dual Camera sensor from one location records the area simultaneously with ten different spectral bands. The MS model with a spatial resolution of 4.14 cm consists of ten separate spectral bands, the order of which can be independently changed and combined to find the best spectral bands layout for the observed objects. DOP was also generated in Agisoft Metashape 1.5.1. using 927 images, yielding a spatial resolution of 1.88 cm.

3.2. GEOBIA

An optimal combination of spectral bands was chosen by visual analysis using the Symbology tool within ArcGIS. The band combination layout 10-9-8 (NIR, RedEdge 740, RedEdge) was chosen as the optimal one due to the possibility of very good differentiation of olive tree crowns compared to other vegetation (Figure 10).



Figure 10. MS model with 10-9-8 bands layout.

3.2.1. Segmentation

By visual interpretation of the generated models, a model with values of spectral detail 18, spatial detail 11, and minimum segment size 15 was selected (Figure 4). The stated values are similar to the values used in research in which the GEOBIA approach to vegetation mapping was applied [13,63,68].

3.2.2. Test Samples

In all, 2946 samples were collected within 14 classes. In addition to the four classes related to olive tree canopies, test samples were added for the class of shadows, classes of anthropogenic objects such as house roofs, macadam and asphalt surfaces, classes of surface karst area and soil with karst, and classes related to canopies of other vegetation types.

3.2.3. Results of Classification Algorithms

The SVM classification algorithm (Figure 11a) enabled distinguishing the class of olive canopies. The majority of the olive trees in the study area are well known in their surroundings. However, there are some shortcomings in the class of other vegetation, where areas that belong to the class of other vegetation are incorrectly classified as olives in some areas. Moreover, the volume of the olive canopies in certain parts is reduced due to the influence of shadows, especially on the axial side of the canopies. Classification algorithm MLC (Figure 11b) classifies and differentiates the shadows much better than the olive tree canopies class. On the other hand, the algorithm recognizes less the differences between the olive class and other vegetation, i.e., it more often classifies olives under the other vegetation class. The RTC algorithm separates the olive canopies class accurately and shows the fewest shortcomings compared to others (Figure 11c). RTC differentiates less well the spatial distribution of classes within the study area. Namely, shadows are very poorly recognized, while surfaces covered with karst are very often classified under the soil class. But, since the object of research are olive tree canopies, RTC ultimately shows very good results.

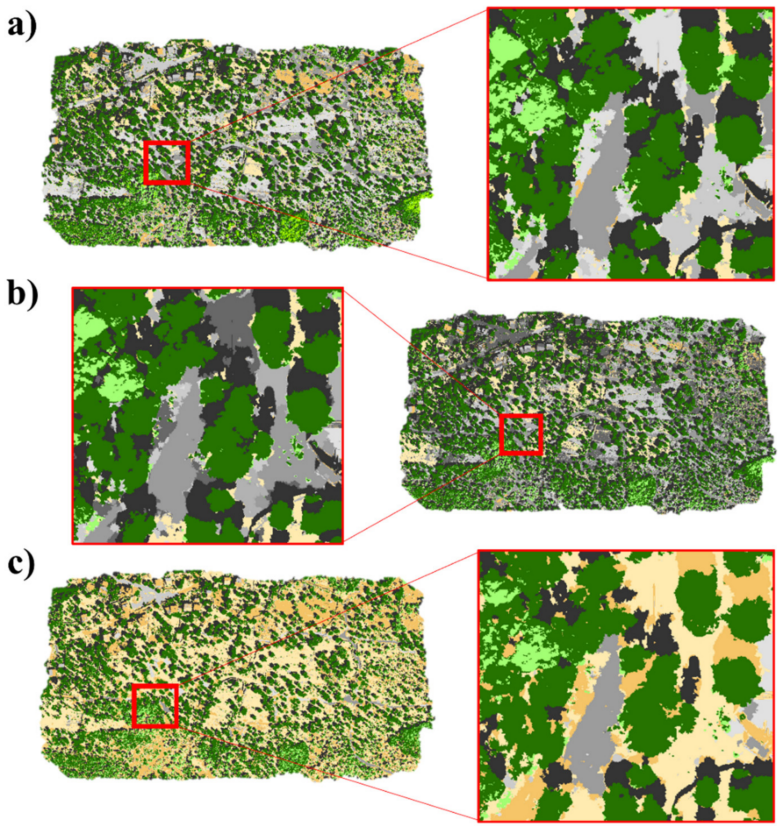


Figure 11. Classified models: (**a**) SVM; (**b**) MLC; (**c**) RTC.

3.2.4. Accuracy of Classification Algorithms

RTC proved to be the most reliable classification algorithm. RTC values (Table 2) produced the best results in three of the four accuracy measures used. The best results were achieved with *UA*, *OA*, and *KC*. The classification algorithm ML in all used measures shows slightly less accurate results compared to RTC. ML shows the least accurate results in *PA*, *UA*, and *KC* values, while it is more reliable than SVM according to *OA*. The SVM classification algorithm shows the least reliable results according to the *OA*, while the best values are related to the *PA*. The results of the accuracy assessment using *UA* and *KC* are in the middle between the results of the two algorithms.

Table 2. GEOBIA accuracy assessment measures results.

Algorithm/Measure	*UA*	*PA*	*OA*	*KC*
RTC	0.8113 0.7378	0.9195 0.5144	0.7565	0.4615
MLC	0.7729 0.7306	0.8997 0.5071	0.7418	0.4311
SVM	0.7511 0.7361	0.8818 0.5302	0.7403	0.4328

Authors in [68] used SVM, MLC, and RTC algorithms to extract coastal coniferous forests, and by accuracy assessment measure KC, the RTC algorithm was selected as the most accurate one. In [69], RTC shows the best performance in object-based land-cover classification. In [63], the most accurate results for olive tree canopies extraction were shown by the SVM classification algorithm with 0.904 results in the AUC measure, while the second one was the MLC algorithm with 0.864. More accurate results in the mentioned study are explainable by greater study area and lower spatial resolution with a GSD of 18 cm for UAV_{MS}.

3.3. Vegetation Indices

3.3.1. Derived VIs Models

The NDVI model (Figure 12a) qualitatively separates areas under vegetation but shows shortcomings in differentiating types of canopies. The NDRE VI model (Figure 12b) distinguishes vegetation and shows olive tree canopies with high reliability. The GNDVI index model (Figure 12c) was chosen due to its ability to distinguish types of vegetation within the study area, while the MCARI2 index model (Figure 12d) reliably distinguishes vegetation surfaces. The last derived model of the RDVI2 index (Figure 12e) was chosen due to its ability to recognize olive trees in relation to other vegetation.

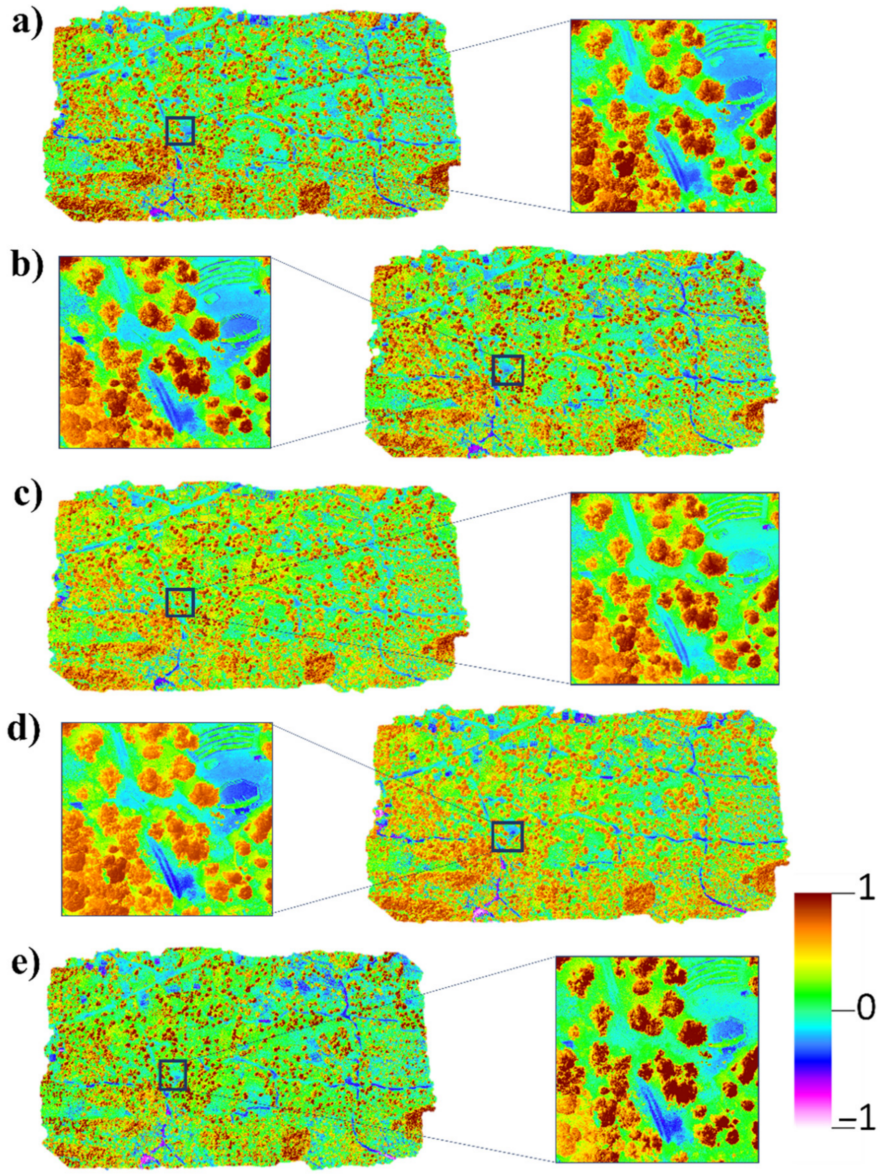


Figure 12. VIs models: (**a**) NDVI; (**b**) NDRE; (**c**) GNDVI; (**d**) MCARI2; (**e**) RDVI2.

3.3.2. VITO Tool Results

The olive tree canopies of five selected VIs were extracted using the VITO tool. The models are classified into the class "olive tree canopies" and the class "other" (Figure 13). Differences in the size and spatial distribution of olive canopy class surfaces vary between VIs, which is expected given the different formulas and spectral bands used when generating the indices.

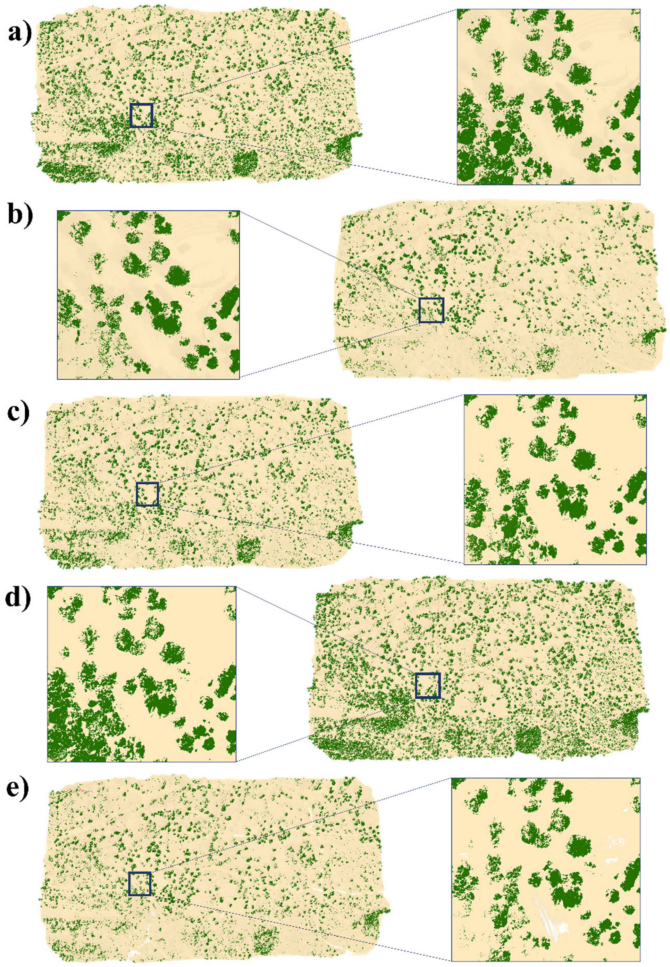


Figure 13. VIs classified models: (**a**) NDVI; (**b**) NDRE; (**c**) GNDVI; (**d**) MCARI2; (**e**) RDVI2.

3.3.3. Accuracy of VIs Models

The most accurate results are shown by the NDRE VI model, while all other models show significantly lower accuracy (Figure 14).

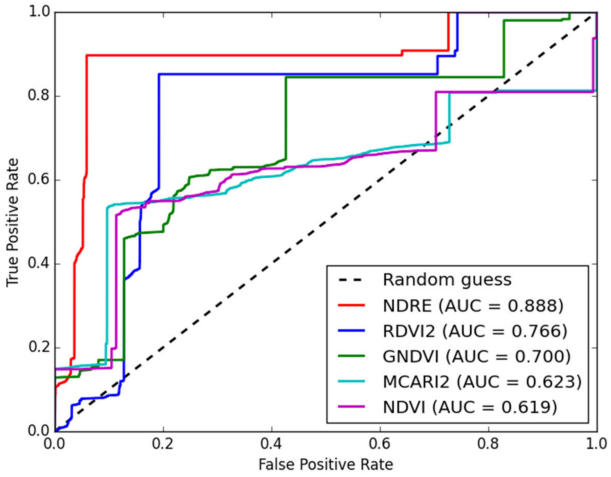


Figure 14. ROC curves and AUC values for VIs models.

The NDRE VI models are often used in many studies involving canopies extraction of different types of vegetation. In [70], the NDRE VI model is used for predicting grain yield in rice, while in [71] it is used for detecting spatial and temporal variations in soybean

crops. Many authors such as [13,40,72] used NDRE as the main VIs model in their studies related to the olive-growing sector. On the other hand, the most used VI for the purpose, the NDVI model [73–75], is showing the least accurate results in this study.

3.4. Results of Used Approaches Comparison

The approach based on VIs shows slightly better results in terms of extracting the olive tree canopies compared to the GEOBIA approach, according to five measures of accuracy. In the method of testing the accuracy with the use of regularly distributed points within the RT and FT, the VIs showed better results in four of the five measures used. According to the measures of AUC (Figure 15), *PA*, *UA*, and *KC*, the approach based on VIs is more accurate, while the GEOBIA approach showed slightly better results only in the measure of *OA* (Table 3).

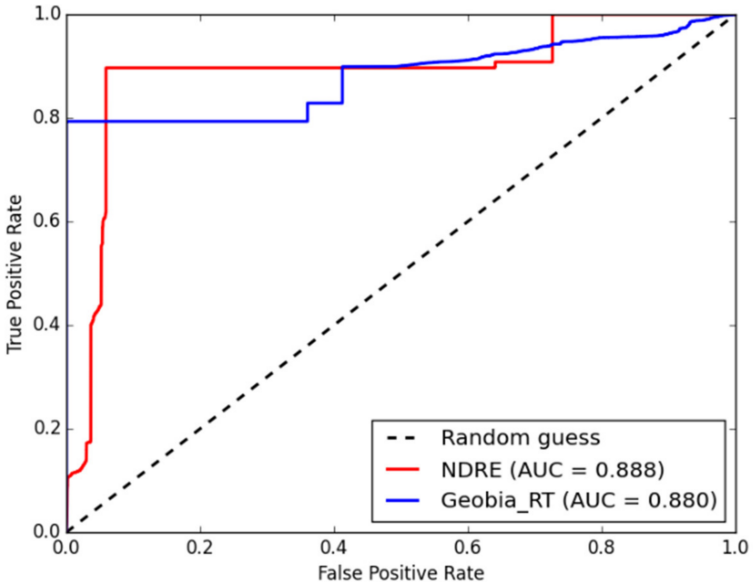


Figure 15. ROC curves and AUC values for RT and FT polygons comparison.

Table 3. Accuracy assessment results for RT and FT polygons comparison.

Algorithm/Measure	*UA*	*PA*	*OA*	*KC*
VIs (NDRE)	0.9388 0.6281	0.9394 0.6257	0.7519	0.5228
GEOBIA (RTC)	0.8113 0.7378	0.9195 0.5144	0.7565	0.4615

The second accuracy check method based on a layer of one thousand randomly distributed points confirms the results obtained by the first method. The results of all five used accuracy measures indicate the selection of the approach based on VIs was more accurate in the extraction of the olive tree canopies than the GEOBIA approach (Table 4) (Figure 16).

Table 4. Accuracy assessment results for 1000 points comparison.

Algorithm/Measure	*UA*	*PA*	*OA*	*KC*
VIs (NDRE)	0.9194 0.9043	0.9893 0.5380	0.9180	0.6311
GEOBIA (RTC)	0.9634 0.4567	0.8135 0.8354	0.8170	0.4855

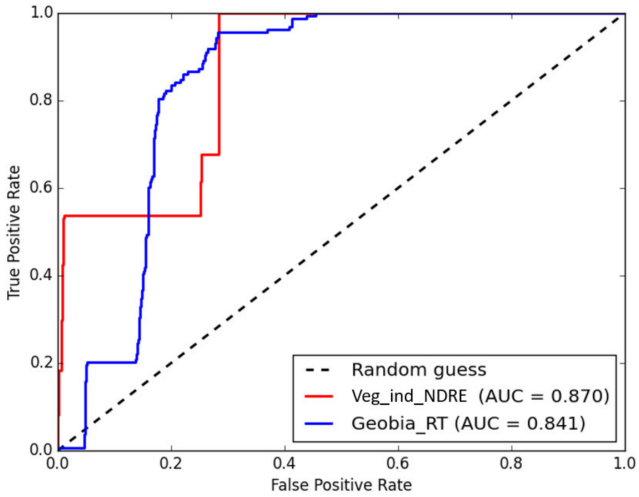


Figure 16. ROC curves and AUC values for 1000 points comparison.

4. Conclusions

Very high-resolution UAV_{MS} was generated for the micro-location within the area of the Lun olive gardens on the island of Pag. Generated UAV_{MS} with a spatial resolution of 4.14 cm was used to generate GEOBIA and VIs models in the olive tree canopies extraction process. In the GEOBIA approach, three classification algorithms were tested, which resulted in choosing the RTC model as the most accurate one (OA = 0.7565), although models SVM (OA = 0.7418) and MLC (OA = 0.7403) showed also very satisfying results. The second approach, which included VIs, showed significantly greater deviations in the accuracy assessment results, with the most accurate NDRE VI model resulting in 0.888 and the NDVI model resulting in 0.619 in the AUC measure. Deviations can be explained mostly due to the different spectral band formulas which were used in the generation process.

In the final comparison, accuracy assessment metrics revealed that the VIs approach is more accurate than the GEOBIA approach in the extraction of olive tree canopies. VI NDRE model showed better results in both compared methods. In the first method which included polygons of RT and FT, the VI NDRE model resulted in 0.888 in AUC and 0.7519 in OA, while GEOBIA RTC resulted in 0.880 in AUC and 0.7565 in OA. The above-mentioned shows that the GEOBIA approach is also very reliable in the olive tree canopies extraction process; but in this study, VIs model showed better results. In conclusion, the GEOBIA method takes a lot of time with all steps combined and the process complexity, while the method with VIs is a very fast and efficient method with accuracy resulting mostly even or higher results than the GEOBIA, an approach created for the purpose.

Author Contributions: Conceptualization, A.Š., I.M. and M.J.; methodology, A.Š., R.M. (Rajko Marinović), F.D., L.P. and R.M. (Rina Milošević); software, A.Š., R.M. (Rajko Marinović), F.D. and R.M. (Rina Milošević); validation, A.Š., L.P., M.J., I.M. and D.R.; formal analysis, A.Š., R.M. (Rajko Marinović) and F.D.; investigation, A.Š., R.M. (Rajko Marinović), L.P. and R.M. (Rina Milošević); resources, A.Š., M.J. and D.R.; data curation, R.M. (Rajko Marinović), F.D., I.M., L.P. and R.M. (Rina Milošević); writing—original draft preparation, A.Š. and R.M. (Rajko Marinović); writing—review and editing, F.D., M.J., L.P. and D.R.; visualization, A.Š., R.M. (Rajko Marinović) and F.D.; supervision, A.Š., M.J., I.M. and D.R.; project administration, M.J., I.M. and D.R.; funding acquisition, A.Š. and M.J. All authors have read and agreed to the published version of the manuscript.

Funding: This research was performed within the project UIP-2017-05-2694, which was financially supported by the Croatian Science Foundation. This research was also funded by the Italy-Croatia cross-border cooperation program 2014–2020 as part of the STREAM (Strategic development of flood management) project.

Institutional Review Board Statement: Not applicable.

Informed Consent Statement: Not applicable.

Data Availability Statement: The data presented in this study are available on request from the corresponding author.

Acknowledgments: This research was produced as part of the project UIP-2017-05-2694 financially supported by the Croatian Science Foundation. Results and findings from this study will be used for further research of the STREAM (Strategic development of flood management) project, funded by the Italy-Croatia cross-border cooperation program 2014–2020. The authors would also like to thank "Lun Olive Grove Garden", and especially Andrea Badurina for his great help during the fieldwork.

Conflicts of Interest: The authors declare no conflict of interest.

References

1. Besnard, G.; Hernández, P.; Khadari, B.; Dorado, G.; Savolainen, V. Genomic Profiling of Plastid DNA Variation in the Mediterranean Olive Tree. *BMC Plant Biol.* **2011**, *11*, 80. [CrossRef] [PubMed]
2. Díez, C.M.; Trujillo, I.; Barrio, E.; Belaj, A.; Barranco, D.; Rallo, L. Centennial Olive Trees as a Reservoir of Genetic Diversity. *Ann. Bot.* **2011**, *108*, 797–807. [CrossRef] [PubMed]
3. Kostelenos, G.; Kiritsakis, A. Olive Tree History and Evolution. In *Olives and Olive Oil as Functional Foods*; John Wiley & Sons, Ltd.: St. John's, NL, Canada, 2017; pp. 1–12. ISBN 978-1-119-13534-0.
4. Potts, S.G.; Petanidou, T.; Roberts, S.; O'Toole, C.; Hulbert, A.; Willmer, P. Plant-Pollinator Biodiversity and Pollination Services in a Complex Mediterranean Landscape. *Biol. Conserv.* **2006**, *129*, 519–529. [CrossRef]
5. Serra, P.; Pons, X.; Saurí, D. Land-Cover and Land-Use Change in a Mediterranean Landscape: A Spatial Analysis of Driving Forces Integrating Biophysical and Human Factors. *Appl. Geogr.* **2008**, *28*, 189–209. [CrossRef]
6. Rodríguez Sousa, A.A.; Barandica, J.M.; Aguilera, P.A.; Rescia, A.J. Examining Potential Environmental Consequences of Climate Change and Other Driving Forces on the Sustainability of Spanish Olive Groves under a Socio-Ecological Approach. *Agriculture* **2020**, *10*, 509. [CrossRef]
7. Fraga, H.; Moriondo, M.; Leolini, L.; Santos, J.A. Mediterranean Olive Orchards under Climate Change: A Review of Future Impacts and Adaptation Strategies. *Agronomy* **2020**, *11*, 56. [CrossRef]
8. Loumou, A.; Giourga, C. Olive Groves: "The Life and Identity of the Mediterranean". *Agric. Hum. Values* **2003**, *20*, 87–95. [CrossRef]
9. Belleti, E.; Bevilaqua, V.R.; Brito, A.M.; Modesto, D.A.; Lanfredi, A.J.; Viviani, V.R.; Nantes-Cardoso, I.L. Synthesis of Bioluminescent Gold Nanoparticle–Luciferase Hybrid Systems for Technological Applications. *Photochem. Photobiol. Sci.* **2021**, *20*, 1439–1453. [CrossRef] [PubMed]
10. Čurović, Ž.; Čurović, M.; Spalević, V.; Janic, M.; Sestras, P.; Popović, S.G. Identification and Evaluation of Landscape as a Precondition for Planning Revitalization and Development of Mediterranean Rural Settlements—Case Study: Mrkovi Village, Bay of Kotor, Montenegro. *Sustainability* **2019**, *11*, 2039. [CrossRef]
11. Hernández-Mogollón, J.M.; Di-Clemente, E.; Campón-Cerro, A.M.; Folgado-Fernández, J.A. Olive Oil Tourism in the Euro-Mediterranean Area. *Int. J. Euro-Mediterr. Stud.* **2021**, *14*, 85–101.
12. Calera, A.; Campos, I.; Osann, A.; D'Urso, G.; Menenti, M. Remote Sensing for Crop Water Management: From ET Modelling to Services for the End Users. *Sensors* **2017**, *17*, 1104. [CrossRef] [PubMed]
13. Solano, F.; Di Fazio, S.; Modica, G. A Methodology Based on GEOBIA and WorldView-3 Imagery to Derive Vegetation Indices at Tree Crown Detail in Olive Orchards. *Int. J. Appl. Earth Obs. Geoinf.* **2019**, *83*, 101912. [CrossRef]
14. Zha, H.; Miao, Y.; Wang, T.; Li, Y.; Zhang, J.; Sun, W.; Feng, Z.; Kusnierek, K. Improving Unmanned Aerial Vehicle Remote Sensing-Based Rice Nitrogen Nutrition Index Prediction with Machine Learning. *Remote Sens.* **2020**, *12*, 215. [CrossRef]
15. Jurišić, M.; Radočaj, D.; Šiljeg, A.; Antonić, O.; Živić, T. Current Status and Perspective of Remote Sensing Application in Crop Management. *J. Cent. Eur. Agric.* **2021**, *22*, 156–166. [CrossRef]
16. Bodzin, A.M.; Cirucci, L. Integrating Geospatial Technologies to Examine Urban Land Use Change: A Design Partnership. *J. Geogr.* **2009**, *108*, 186–197. [CrossRef]
17. Jackson, M.; Schell, D.; Taylor, D.F. The Evolution of Geospatial Technology Calls for Changes in Geospatial Research, Education and Government Management. *Dir. Mag.* **2009**, *13*, 1–9.
18. Bishop, M.P.; James, L.A.; Shroder Jr, J.F.; Walsh, S.J. Geospatial Technologies and Digital Geomorphological Mapping: Concepts, Issues and Research. *Geomorphology* **2012**, *137*, 5–26. [CrossRef]
19. Marques, P.; Pádua, L.; Adão, T.; Hruška, J.; Peres, E.; Sousa, A.; Sousa, J.J. UAV-Based Automatic Detection and Monitoring of Chestnut Trees. *Remote Sens.* **2019**, *11*, 855. [CrossRef]
20. Ballesteros, R.; Ortega, J.F.; Hernández, D.; Moreno, M.A. Applications of Georeferenced High-Resolution Images Obtained with Unmanned Aerial Vehicles. Part I: Description of Image Acquisition and Processing. *Precis. Agric.* **2014**, *15*, 579–592. [CrossRef]
21. Ronchetti, G.; Mayer, A.; Facchi, A.; Ortuani, B.; Sona, G. Crop Row Detection through UAV Surveys to Optimize On-Farm Irrigation Management. *Remote Sens.* **2020**, *12*, 1967. [CrossRef]
22. Martínez-Casasnovas, J.A.; Sandonís-Pozo, L.; Escolà, A.; Arnó, J.; Llorens, J. Delineation of Management Zones in Hedgerow Almond Orchards Based on Vegetation Indices from UAV Images Validated by LiDAR-Derived Canopy Parameters. *Agronomy* **2021**, *12*, 102. [CrossRef]

23. Hobart, M.; Pflanz, M.; Weltzien, C.; Schirrmann, M. Growth Height Determination of Tree Walls for Precise Monitoring in Apple Fruit Production Using UAV Photogrammetry. *Remote Sens.* **2020**, *12*, 1656. [CrossRef]
24. Šiljeg, A.; Domazetović, F.; Marić, I.; Pandja, L. Quality Assessment of Worldview-3 Stereo Imagery Derived Models Over Millennial Olive Groves. In *International Conference on Geographical Information Systems Theory, Applications and Management*; Springer: Cham, Switzerland, 2020; pp. 66–84.
25. Zhang, W.; Gao, F.; Jiang, N.; Zhang, C.; Zhang, Y. High-Temporal-Resolution Forest Growth Monitoring Based on Segmented 3D Canopy Surface from UAV Aerial Photogrammetry. *Drones* **2022**, *6*, 158. [CrossRef]
26. Stateras, D.; Kalivas, D. Assessment of Olive Tree Canopy Characteristics and Yield Forecast Model Using High Resolution UAV Imagery. *Agriculture* **2020**, *10*, 385. [CrossRef]
27. Jurado, J.M.; Ortega, L.; Cubillas, J.J.; Feito, F.R. Multispectral Mapping on 3D Models and Multi-Temporal Monitoring for Individual Characterization of Olive Trees. *Remote Sens.* **2020**, *12*, 1106. [CrossRef]
28. Martinelli, F.; Scalenghe, R.; Davino, S.; Panno, S.; Scuderi, G.; Ruisi, P.; Villa, P.; Stroppiana, D.; Boschetti, M.; Goulart, L.R. Advanced Methods of Plant Disease Detection. A Review. *Agron. Sustain. Dev.* **2015**, *35*, 1–25. [CrossRef]
29. Sullivan, J.M. Evolution or Revolution? The Rise of UAVs. *IEEE Technol. Soc. Mag.* **2006**, *25*, 43–49. [CrossRef]
30. Ozdemir, U.; Aktas, Y.O.; Vuruskan, A.; Dereli, Y.; Tarhan, A.F.; Demirbag, K.; Erdem, A.; Kalaycioglu, G.D.; Ozkol, I.; Inalhan, G. Design of a Commercial Hybrid VTOL UAV System. *J. Intell. Robot Syst.* **2014**, *74*, 371–393. [CrossRef]
31. Alvarez-Vanhard, E.; Corpetti, T.; Houet, T. UAV & Satellite Synergies for Optical Remote Sensing Applications: A Literature Review. *Sci. Remote Sens.* **2021**, *3*, 100019. [CrossRef]
32. Sozzi, M.; Kayad, A.; Gobbo, S.; Cogato, A.; Sartori, L.; Marinello, F. Economic Comparison of Satellite, Plane and UAV-Acquired NDVI Images for Site-Specific Nitrogen Application: Observations from Italy. *Agronomy* **2021**, *11*, 2098. [CrossRef]
33. Watts, A.C.; Ambrosia, V.G.; Hinkley, E.A. Unmanned Aircraft Systems in Remote Sensing and Scientific Research: Classification and Considerations of Use. *Remote Sens.* **2012**, *4*, 1671–1692. [CrossRef]
34. Pádua, L.; Vanko, J.; Hruška, J.; Adão, T.; Sousa, J.J.; Peres, E.; Morais, R. UAS, Sensors, and Data Processing in Agroforestry: A Review towards Practical Applications. *Int. J. Remote Sens.* **2017**, *38*, 2349–2391. [CrossRef]
35. Delavarpour, N.; Koparan, C.; Nowatzki, J.; Bajwa, S.; Sun, X. A Technical Study on UAV Characteristics for Precision Agriculture Applications and Associated Practical Challenges. *Remote Sens.* **2021**, *13*, 1204. [CrossRef]
36. Minařík, R.; Langhammer, J. Use of a Multispectral Uav Photogrammetry for Detection and Tracking of Forest Disturbance Dynamics. *ISPRS Int. Arch. Photogramm. Remote Sens. Spat. Inf. Sci.* **2016**, *XLI-B8*, 711–718. [CrossRef]
37. Fernández-Lozano, J.; Sanz-Ablanedo, E. Unraveling the Morphological Constraints on Roman Gold Mining Hydraulic Infrastructure in NW Spain. A UAV-Derived Photogrammetric and Multispectral Approach. *Remote Sens.* **2021**, *13*, 291. [CrossRef]
38. Stow, D.; Hope, A.; Nguyen, A.T.; Phinn, S.; Benkelman, C.A. Monitoring Detailed Land Surface Changes Using an Airborne Multispectral Digital Camera System. *IEEE Trans. Geosci. Remote Sens.* **1996**, *34*, 1191–1203. [CrossRef]
39. Iqbal, F.; Lucieer, A.; Barry, K. Simplified Radiometric Calibration for UAS-Mounted Multispectral Sensor. *Eur. J. Remote Sens.* **2018**, *51*, 301–313. [CrossRef]
40. Avola, G.; Di Gennaro, S.F.; Cantini, C.; Riggi, E.; Muratore, F.; Tornambè, C.; Matese, A. Remotely Sensed Vegetation Indices to Discriminate Field-Grown Olive Cultivars. *Remote Sens.* **2019**, *11*, 1242. [CrossRef]
41. Huete, A.R. Vegetation Indices, Remote Sensing and Forest Monitoring. *Geogr. Compass* **2012**, *6*, 513–532. [CrossRef]
42. Messina, G.; Fiozzo, V.; Praticò, S.; Siciliani, B.; Curcio, A.; Di Fazio, S.; Modica, G. Monitoring Onion Crops Using Multispectral Imagery from Unmanned Aerial Vehicle (UAV). In *New Metropolitan Perspectives*; Bevilacqua, C., Calabrò, F., Della Spina, L., Eds.; Springer International Publishing: Cham, Switzerland, 2021; pp. 1640–1649.
43. Perry, C.R.; Lautenschlager, L.F. Functional Equivalence of Spectral Vegetation Indices. *Remote Sens. Environ.* **1984**, *14*, 169–182. [CrossRef]
44. Jackson, R.D.; Huete, A.R. Interpreting Vegetation Indices. *Prev. Vet. Med.* **1991**, *11*, 185–200. [CrossRef]
45. Bannari, A.; Morin, D.; Bonn, F.; Huete, A.R. A Review of Vegetation Indices. *Remote Sens. Rev.* **1995**, *13*, 95–120. [CrossRef]
46. Baret, F.; Guyot, G. Potentials and Limits of Vegetation Indices for LAI and APAR Assessment. *Remote Sens. Environ.* **1991**, *35*, 161–173. [CrossRef]
47. Xue, J.; Su, B. Significant Remote Sensing Vegetation Indices: A Review of Developments and Applications. *J. Sens.* **2017**, *2017*, e1353691. [CrossRef]
48. Candiago, S.; Remondino, F.; De Giglio, M.; Dubbini, M.; Gattelli, M. Evaluating Multispectral Images and Vegetation Indices for Precision Farming Applications from UAV Images. *Remote Sens.* **2015**, *7*, 4026–4047. [CrossRef]
49. Blaschke, T.; Hay, G.J.; Kelly, M.; Lang, S.; Hofmann, P.; Addink, E.; Queiroz Feitosa, R.; van der Meer, F.; van der Werff, H.; van Coillie, F.; et al. Geographic Object-Based Image Analysis—Towards a New Paradigm. *ISPRS J. Photogramm. Remote Sens.* **2014**, *87*, 180–191. [CrossRef] [PubMed]
50. Chen, G.; Weng, Q.; Hay, G.J.; He, Y. Geographic Object-Based Image Analysis (GEOBIA): Emerging Trends and Future Opportunities. *GIScience Remote Sens.* **2018**, *55*, 159–182. [CrossRef]
51. Hay, G.J.; Castilla, G. Geographic Object-Based Image Analysis (GEOBIA): A New Name for a New Discipline. In *Object-Based Image Analysis: Spatial Concepts for Knowledge-Driven Remote Sensing Applications*; Lecture Notes in Geoinformation and Cartography; Blaschke, T., Lang, S., Hay, G.J., Eds.; Springer: Berlin/Heidelberg, Germany, 2008; pp. 75–89. ISBN 978-3-540-77058-9.

52. Grinblat, G.L.; Uzal, L.C.; Larese, M.G.; Granitto, P.M. Deep Learning for Plant Identification Using Vein Morphological Patterns. *Comput. Electron. Agric.* **2016**, *127*, 418–424. [CrossRef]
53. LeCun, Y.; Bengio, Y.; Hinton, G. Deep Learning. *Nature* **2015**, *521*, 436–444. [CrossRef]
54. Jozdani, S.E.; Johnson, B.A.; Chen, D. Comparing Deep Neural Networks, Ensemble Classifiers, and Support Vector Machine Algorithms for Object-Based Urban Land Use/Land Cover Classification. *Remote Sens.* **2019**, *11*, 1713. [CrossRef]
55. Milotić, I. The Ownership of Olive Trees in Lun (Island Pag) and the Principle superficies solo cedit. *Zb. Pravnog Fak. U Zagreb.* **2013**, *63*, 1319–1350.
56. Connor, D.J.; Fereres, E. The Physiology of Adaptation and Yield Expression in Olive. In *Horticultural Reviews*; Janick, J., Ed.; John Wiley & Sons, Inc.: Oxford, UK, 2010; pp. 155–229. ISBN 978-0-470-65088-2.
57. Geerling, G.W.; Labrador-Garcia, M.; Clevers, J.G.P.W.; Ragas, A.M.J.; Smits, A.J.M. Classification of Floodplain Vegetation by Data Fusion of Spectral (CASI) and LiDAR Data. *Int. J. Remote Sens.* **2007**, *28*, 4263–4284. [CrossRef]
58. Congalton, R.G. A Review of Assessing the Accuracy of Classifications of Remotely Sensed Data. *Remote Sens. Environ.* **1991**, *37*, 35–46. [CrossRef]
59. Liu, C.; Frazier, P.; Kumar, L. Comparative Assessment of the Measures of Thematic Classification Accuracy. *Remote Sens. Environ.* **2007**, *107*, 606–616. [CrossRef]
60. Thompson, W.D.; Walter, S.D. A Reappraisal of the kappa coefficient. *J. Clin. Epidemiol.* **1988**, *41*, 949–958. [CrossRef]
61. Rigby, A.S. Statistical Methods in Epidemiology. v. Towards an Understanding of the Kappa Coefficient. *Disabil. Rehabil.* **2000**, *22*, 339–344. [CrossRef]
62. Koukoulas, S.; Blackburn, G.A. Mapping Individual Tree Location, Height and Species in Broadleaved Deciduous Forest Using Airborne LIDAR and Multi-spectral Remotely Sensed Data. *Int. J. Remote Sens.* **2005**, *26*, 431–455. [CrossRef]
63. Šiljeg, A.; Panđa, L.; Domazetović, F.; Marić, I.; Gašparović, M.; Borisov, M.; Milošević, R. Comparative Assessment of Pixel and Object-Based Approaches for Mapping of Olive Tree Crowns Based on UAV Multispectral Imagery. *Remote Sens.* **2022**, *14*, 757. [CrossRef]
64. Bradley, A.P. The Use of the Area under the ROC Curve in the Evaluation of Machine Learning Algorithms. *Pattern Recognit.* **1997**, *30*, 1145–1159. [CrossRef]
65. Krzanowski, W.J.; Hand, D.J. *ROC Curves for Continuous Data*; Chapman and Hall/CRC: New York, NY, USA, 2009; ISBN 978-0-429-16610-5.
66. Hand, D.J. A Simple Generalisation of the Area Under the ROC Curve for Multiple Class Classification Problems. *Mach. Learn.* **2001**, *45*, 171–186. [CrossRef]
67. Narkhede, S. Understanding AUC-ROC Curve. *Towards Data Sci.* **2018**, *26*, 220–227.
68. Panđa, L.; Milošević, R.; Šiljeg, S.; Domazetović, F.; Marić, I.; Šiljeg, A. Comparison of GEOBIA classification algorithms based on Worldview-3 imagery in the extraction of coastal coniferous forest. *Šumar. List (Online)* **2021**, *145*, 535–544. [CrossRef]
69. Ma, L.; Li, M.; Ma, X.; Cheng, L.; Du, P.; Liu, Y. A Review of Supervised Object-Based Land-Cover Image Classification. *ISPRS J. Photogramm. Remote Sens.* **2017**, *130*, 277–293. [CrossRef]
70. Zhou, X.; Zheng, H.B.; Xu, X.Q.; He, J.Y.; Ge, X.K.; Yao, X.; Cheng, T.; Zhu, Y.; Cao, W.X.; Tian, Y.C. Predicting Grain Yield in Rice Using Multi-Temporal Vegetation Indices from UAV-Based Multispectral and Digital Imagery. *ISPRS J. Photogramm. Remote Sens.* **2017**, *130*, 246–255. [CrossRef]
71. Morlin Carneiro, F.; Angeli Furlani, C.E.; Zerbato, C.; Candida de Menezes, P.; da Silva Gírio, L.A.; Freire de Oliveira, M. Comparison between Vegetation Indices for Detecting Spatial and Temporal Variabilities in Soybean Crop Using Canopy Sensors. *Precis. Agric* **2020**, *21*, 979–1007. [CrossRef]
72. Jorge, J.; Vallbé, M.; Soler, J.A. Detection of Irrigation Inhomogeneities in an Olive Grove Using the NDRE Vegetation Index Obtained from UAV Images. *Eur. J. Remote Sens.* **2019**, *52*, 169–177. [CrossRef]
73. Gitelson, A.A.; Kaufman, Y.J.; Merzlyak, M.N. Use of a Green Channel in Remote Sensing of Global Vegetation from EOS- MODIS. *Remote Sens. Environ.* **1996**, *58*, 289–298. [CrossRef]
74. Patón, D. Normalized Difference Vegetation Index Determination in Urban Areas by Full-Spectrum Photography. *Ecologies* **2020**, *1*, 22–35. [CrossRef]
75. Huang, S.; Tang, L.; Hupy, J.P.; Wang, Y.; Shao, G. A Commentary Review on the Use of Normalized Difference Vegetation Index (NDVI) in the Era of Popular Remote Sensing. *J. For. Res.* **2021**, *32*, 1–6, Erratum in *J. For. Res.* **2021**, *32*, 2719. [CrossRef]

Disclaimer/Publisher's Note: The statements, opinions and data contained in all publications are solely those of the individual author(s) and contributor(s) and not of MDPI and/or the editor(s). MDPI and/or the editor(s) disclaim responsibility for any injury to people or property resulting from any ideas, methods, instructions or products referred to in the content.